Science, Engineering and Technology Vol. 6, No. 1, pp. 98-122
www.setjournal.com https://doi.org/10.54327/set2026/v6.i1.317

Experimental Study of the Combined Effects of Operating Parameters of a Diesel Engine under Increasing Exhaust Backpressure Conditions

Nhlanhla Khanyi, Riaan Stopforth

Department of Mechanical Engineering, School of Engineering, University of Kwa-Zulu Natal, Durban 4041, South Africa.

Abstract

Diesel engines remain widely used in transportation and power generation due to their high efficiency and durability. However, their combustion behaviour, performance, and emissions are strongly influenced by operating conditions such as exhaust backpressure (EBP). This study experimentally investigates the combined effects of compression ratio (CR), engine load, and EBP on combustion characteristics, thermal performance, heat transfer, and emissions of a diesel engine operating at 1 500 rpm. Results show that moderate CR values (14–16) and engine loads of 50–75% enhance in-cylinder pressure, heat release rate, and combustion efficiency. In contrast, excessive CR (18) and high EBP (60 kPa) increase in-cylinder temperature and residual gas fraction (RGF), leading to reduced heat release rates and longer ignition delay. The highest brake thermal efficiency (approximately 33%) is achieved at moderate load and low EBP, whereas high CR and load under elevated EBP reduce efficiency and increase brake-specific fuel consumption. Heat transfer analysis indicates that excessive CR and load significantly raise thermal loads, emphasizing the need for accurate predictive correlations in engine design. Emissions analysis reveals minimal CO and HC at moderate conditions, while NOx and smoke increase under extreme operating regimes. Overall, the findings identify an optimal operating window (CR 14–16, 50–75% load, EBP ≤45 kPa) and provide practical guidance for diesel engine under backpressure constraints, contributing to improved efficiency and emissions control.

Keywords*:* diesel engine, combustion, emissions, exhaust backpressure, compression ratio, load.

1. Introduction

Diesel engines are widely used internal combustion (IC) engines that operate on the principle of compression ignition (CI). In this process, air is compressed to high pressure and temperature, after which fuel is directly injected into the combustion chamber, resulting in auto-ignition without the need for an external spark. This operating principle enables high thermal efficiency, durability, and suitability for heavy-duty transportation and stationary power generation applications. Diesel engine combustion behaviour, performance, and emissions are governed by several interacting parameters, including compression ratio (CR), engine load, speed, fuel properties, and exhaust backpressure (EBP) [1].

Increasing the compression ratio (CR) generally raises in-cylinder pressure and temperature, which shortens the ignition delay and enhances heat release rates (HRR). As a result, brake thermal efficiency (BTE) improves while brake-specific fuel consumption (BSFC) decreases. Engine load and speed further influence air–fuel mixing, combustion phasing, and peak cylinder conditions [2], [3]. In addition, alternative fuels such as biodiesel blends modify in-cylinder combustion due to variations in cetane number, viscosity, and calorific value, typically reducing carbon monoxide (CO) and hydrocarbon (HC) emissions but potentially increasing nitrogen oxides (NOx) [4].

In recent years, increasingly stringent global emission regulations have driven the widespread adoption of

Corresponding author: Nhlanhla Khanyi (khanyinf93@gmail.com)
Received: 26 October 2025; Revised: 26 February 2026; Accepted: 5 March 2026; Published: 1 April 2026

exhaust aftertreatment systems in CI engines, including diesel oxidation catalysts (DOC), diesel particulate filters (DPF), selective catalytic reduction (SCR), and ammonia oxidation catalysts (AOC). While these systems are effective in reducing regulated emissions, their integration progressively increases exhaust flow resistance, leading to increased EBP. Higher EBP can disrupt exhaust removal, increase residual gas fraction (RGF), and alter in-cylinder thermodynamic conditions, thereby affecting combustion efficiency, performance, and emissions [5], [6].

Beyond passive increases in EBP, modern CI engines increasingly employ active exhaust flow control strategies, such as exhaust throttle valves, particularly for exhaust thermal management. Under low-load or idling conditions, exhaust gas temperatures (EGT) may be insufficient for optimal catalyst activity. In such cases, controlled elevation of EBP through exhaust throttling increases EGT, improving aftertreatment efficiency and enabling faster catalyst light-off. However, excessive or poorly managed EBP can adversely impact ignition delay, HRR, thermal loading, and fuel consumption. Consequently, understanding the combined influence of CR, load, and regulated EBP is increasingly critical for improving diesel engine performance, durability, and emissions compliance under modern operating and regulatory constraints.

1.1. Related work

Numerous studies have Numerous studies have investigated the performance and emissions characteristics of diesel engines. The widespread adoption of exhaust after-treatment devices to reduce regulated emissions has introduced additional flow resistance in the exhaust system. This resistance often leads to increased EBP, which can adversely influence engine performance and emissions [7]. Consequently, recent research has focused on understanding the effects of EBP under different operating conditions, including variations in engine load, speed, and CR. Some studies have also examined the role of biodiesel blends and their potential to mitigate the adverse effects associated with elevated EBP.

Ma et al. [8] experimentally investigated a diesel engine operating under high EBP generated using a butterfly valve installed in the exhaust pipeline. Their results showed that increasing EBP led to a significant reduction in power output. When the engine load was increased to 75%, partial recovery in power output was observed, indicating that load adjustment can mitigate some negative effects of EBP. Other studies have suggested that modifying the CR under similar conditions could further enhance power output [9], [10], [11]. Joardder et al. [12] examined the performance and emissions of a CI engine across different speeds (600 rpm, 950 rpm, and 1 200 rpm) and loads under varying EBPs ranging from 0 to 80 mm Hg. Their findings indicated that an exhaust back pressure (EBP) of up to 40 mm Hg caused negligible changes in engine performance and emissions under all operating conditions. However, at 80 mm Hg, slight deterioration was observed, suggesting that adverse effects become noticeable once a threshold EBP level is exceeded.

Desale et al. [13] similarly investigated the influence of EBP on a four-cylinder turbocharged diesel engine operating under loads ranging from 40% to 100%. A manually operated gate valve and a differential mercury manometer were used to generate and measure EBP. Their results showed that brake thermal efficiency (BTE) and brake-specific fuel consumption (BSFC) remained largely unchanged with increasing EBP up to 12 mm Hg. Together, the findings of Joardder et al. [12] and Desale et al. [13] demonstrate that moderate EBP levels do not significantly impair CI engine performance. At higher EBP levels, more pronounced adverse effects have been reported. Ebrahimnataj et al. [14] conducted combined numerical and experimental investigations and found that increasing EBP from 3 to 22 kPa resulted in a 7% increase in BSFC when additional fuel was injected. This operating condition was also associated with a 6% reduction in brake power and torque, along with slight increases in CO, HC, and smoke opacity.

Huang et al. [15] studied medium-speed marine diesel engines operating under EBP levels of 10 and 25 kPa across load conditions ranging from 25% to 100%. Their results indicated that increasing EBP had only a minor effect on heat release rate (HRR) and engine power, suggesting that moderate EBP levels may not substantially degrade engine performance. Nevertheless, as shown in earlier studies [12], [13], the negative effects of EBP become increasingly significant as backpressure rises beyond moderate levels, depending on engine operating

conditions. Further evidence of the detrimental impact of high EBP was provided by Gülmez and Özmen [16], who examined diesel engine performance and emissions at a constant speed of 1 600 rpm under various torque loads. Their results showed that brake-specific fuel consumption (BSFC) increased by approximately 3.29% at an exhaust back pressure (EBP) of 24.66 kPa. In addition, higher torque loads combined with elevated EBP resulted in increased hydrocarbon (HC) and carbon monoxide (CO) emissions, supporting the trends reported by Ebrahimnataj et al. [14].

While numerous studies have investigated the effects of varying CR on engine performance and emissions, most have not accounted for the influence of EBP. Renish et al. [17] examined sea mango oil biodiesel blends and diesel fuel under CRs ranging from 16:1 to 18:1 and different load conditions. Their findings showed improved performance and combustion characteristics at higher CRs; however, these results were obtained under the assumption of negligible EBP. Similarly, Costa and Sodré [18] reported improved performance with increasing CR in ethanol–gasoline-fuelled engines across a wide speed range. Shaik et al. [19] investigated the combined effects of CR and exhaust gas recirculation (EGR) in a diesel engine fuelled with a B20 biodiesel blend. They reported increased BTE and reduced CO, HC, and smoke emissions at a CR of 22:1, although NOx emissions increased significantly. The application of EGR at the same CR effectively reduced NOx emissions, highlighting the complex interaction between combustion parameters.

Additional studies have reported similar trends. More et al. [20] observed that higher CRs reduced NOx emissions, while lower CRs were more effective in reducing CO emissions. Polat [21] reported that BSFC generally increased with CR under varying load conditions, although reductions were observed at lower loads beyond a CR of 22. Singh and Shukla [22] showed that increasing CR shortened ignition delay and enhanced cylinder pressure and mean gas temperature, while reducing the heat release rate. Balasubramanian and Subramanian [23] examined the influence of CR at high load conditions and reported improved BTE at a CR of 21, accompanied by increased NOx emissions due to elevated combustion temperatures. Slight increases in HC emissions were also observed and attributed to changes in combustion chamber geometry. Similar trends were reported by Kannan et al. [24], who found that a CR of 19 improved BTE and BSFC but resulted in higher exhaust emissions.

Table 1 summarizes findings from other previous studies on the negative effects of EBP on diesel engine combustion, emissions, and efficiency. To date, the study by Khanyi et al. [25] remains the only work that explicitly examined the interaction between CR and EBP. Their numerical investigation using a variable compression ratio (VCR) diesel engine demonstrated that the benefits of increasing CR were entirely negated under excessive EBP conditions. However, their study did not consider variations in load, engine speed, or fuel type.

Table 1. Summary of exhaust backpressure effects.

Parameter	Observed effect of EBP	Underlying mechanism
Combustion	Delayed ignition and reduced heat release rate	Higher RFG lowers oxygen concentration and slows combustion kinetics [26], [27].
Performance & Efficiency	Reduced brake power and brake thermal efficiency; increased BSFC	Increased pumping losses and reduced effective expansion work [13], [24].
CO & HC Emissions	Higher emissions	Incomplete combustion due to oxygen dilution and reduced flame propagation [19], [20].
NOx Emissions	Higher emissions under high load	Increased in-cylinder temperature and longer residence time promote thermal NOx formation [11], [12].
Soot/Smoke Emissions	Higher opacity and particulate formation	Limited soot oxidation caused by oxygen deficiency and poor exhaust scavenging [33], [35].

Overall, the existing literature highlights the individual effects of CR, load, speed, and fuel properties on diesel engine performance and emissions, while underscoring the need for experimental studies that examine their combined influence under elevated EBP. Addressing this gap is essential for developing strategies that minimize the adverse effects of EBP while preserving the performance and emissions benefits associated with higher CRs and engine loads.

1.2. Research gap, contribution and significance

Despite extensive research on diesel engine performance and emissions, existing studies have largely examined the effects of CR, load, engine speed, and biodiesel blends individually, with limited attention to their interactions under excessive EBP. While some work has considered CR or biodiesel blends, these analyses typically assume negligible EBP, and even studies acknowledging EBP have not systematically assessed its combined effects with multiple operating parameters. This gap raises critical questions about whether the performance benefits of CR and biodiesel blends persist under resistive EBP conditions and highlights the need for a comprehensive, integrated evaluation.

This study addresses this gap by providing the first experimental dataset and analysis of the simultaneous effects of CR, engine load, and EBP on combustion, performance, emissions, and heat transfer characteristics. It identifies optimum operating conditions that balance efficiency and emissions under varying and excessive EBP and incorporates heat transfer considerations. In addition, it introduces a modified Arrhenius equation for improved ignition delay prediction.

The novelty of this work lies in its systematic factorial, multi-factor approach to experimentally investigate the multi-parameter interactions under challenging operating conditions, advancing understanding beyond single-parameter studies. By revealing the combined influence of CR, load, and EBP, the study informs strategies to sustain combustion stability, engine efficiency, and emissions compliance despite the resistive effects of EBP. These insights are critical for guiding both future research and practical engine design in an era of increasing reliance on exhaust after-treatment systems.

2. Materials and Methods

2.1. Experimental set up

This experimental study employed a computerized single-cylinder, 4-stroke, VCR diesel engine to investigate its performance and emission characteristics under fluctuating EBPs. The test rig and experimental setup are illustrated in Figure 1 and Figure 2. The specifications on this diesel engine are summarised in Table 1. The diesel engine utilized conventional diesel fuel and was equipped with an eddy current dynamometer to facilitate engine loading. The engine was equipped with a VCR mechanism that allowed the CR to be adjusted using a dedicated CR adjustment knob integrated into the engine (see Figure 2). During the experiments, the CR was sequentially varied from 12 to 14, 16, and finally 18, enabling the investigation of engine performance and combustion behaviour under different operating conditions.

Figure 1. VCR diesel engine test rig.

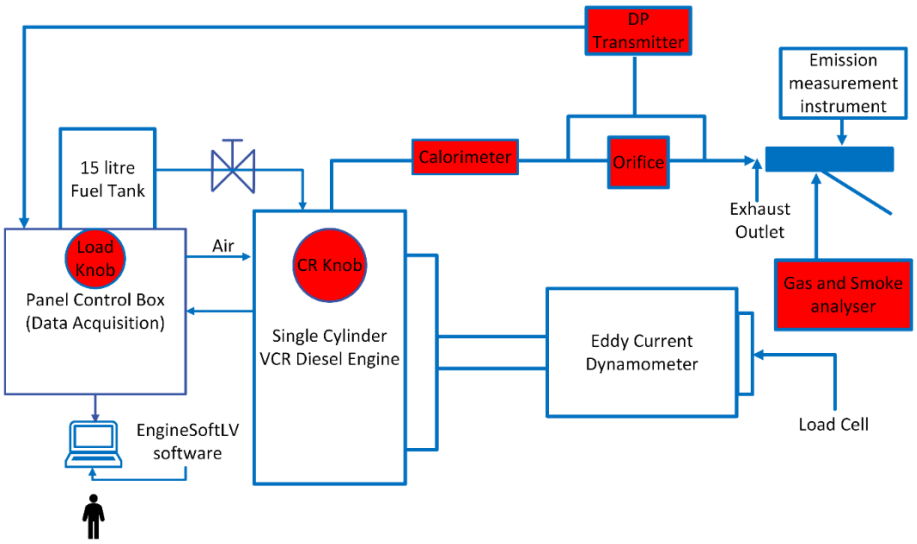

Figure 2. Experimental setup.

The engine was equipped with a piezo sensor to control diesel fuel injection with high precision. To accurately quantify energy losses through exhaust gases, the engine consisted of an exhaust gas calorimeter to measure the heat content of the exhaust gases. An exhaust 1601 combined PUC gas analyzer and AVL 437c smoke meter were also employed to conduct emission analyses, providing insight into the engine's environmental performance. To generate EBP, orifice plates of varying diameters were installed at strategic locations within the exhaust pipeline. The resulting pressure differential between the unrestricted and restricted exhaust sections was recorded by a Rosemount 3051S Series DP transmitter and transmitted to the control unit for continuous monitoring and analysis.

The entire setup was controlled via a standalone panel box which consisted of an air box, a 15-liter fuel tank, and a load controller for adjusting engine load. Fuel consumption was measured using a burette tube (fuel sensor). The water flow rates for both the engine and calorimeter were monitored with rotameters. The panel also included transmitters for airflow and fuel flow measurements, process and engine indicators for actual monitoring, and a manometer to measure the airflow rate into the engine. Furthermore, the panel box integrated a data acquisition system connected to a computer running EnginesoftLV 6.0 software. This system enabled the extraction of various parameters, including EGT, in-cylinder pressure, temperature, and engine performance indicators during the experiments. The specifications of the proposed single cylinder 4-stroke diesel engine are detailed in Table 2 and specification all instruments used in this work are detailed in Table 3, ensuring precise and reliable data collection throughout the experimental procedure.

Table 2. Specifications of the proposed single cylinder 4-stroke diesel engine.

Engine parameters	**Units**	**Values**
Make		Kirloskar
Type		1-cylinder, 4-stroke, VCR diesel, water cooled
Rated power	kW	3.5
Speed	Rpm	1 500
Bore Diameter	Mm	87.5
Stroke	Mm	110
Connecting rod	Mm	234
Compression ratio		Variable (12-18)

Table 3. Specification of the measuring instruments.

Description	Specification
Dynamometer	Type eddy current, water cooled, with loading unit
Piezo sensor	Make PCB USA, Combustion: Range 5 000 PSI, with low noise cable
Combined PUC gas analyser Smoke meter	LCD display type, response time of 5s, and measuring gas intake 1Litre/min AVL 437c
Orifice plates	Stainless steel 304
DP transmitter	Rosemount 3051S Series, DP range 0 to 250 kPa
Data acquisition device	Make NI Instrument USA, NI USB-6210, 16-bit, 250 kS/s
Temperature sensor	Make Radix, Type RTD, PT100 and Thermocouple, Type K
Load indicator	Digital, Range 0 Kg to 50 Kg, Supply 230 VAC
Load sensor	Load cell, type strain gauge, range 0 Kg to 50 Kg
Software	EnginesoftLV 6.0
Rotameter	Engine cooling 40 LPH to 400 LPH; calorimeter 25 LPH to 250 LPH

Uncertainty analysis was conducted to estimate the measurement errors associated with the experimental parameters. In any experimental investigation, a certain level of uncertainty is unavoidable due to factors such as environmental conditions, sensor resolution, calibration procedures, signal processing, and operational variations. Accounting for these uncertainties allows for a more reliable interpretation of the measured data and derived performance parameters. The uncertainty associated with each measured variable was estimated based on the manufacturer's specified instrument accuracy and measurement resolution. Table 4 presents the measuring range, accuracy, and estimated uncertainty for each instrument used in the experimental setup.

Table 4. Range, accuracy, and uncertainty of the instruments.

Equipment	Measured quantity	Measuring range	Accuracy	Uncertainty
Eddy Current Dynamometer	BP	–	$\pm$ 0.03kW	$\pm$ 1.1%
PUC gas analyser	HC CO PM NOx	0 to 500 ppm 0 to 10% vol 0 to 20 000 ppm 0 to 4 800 ppm	$\pm$ 1.25% $\pm$ 0.03% $\pm$ 0.01vol% $\pm$ 20ppm	$\pm$ 0.15% $\pm$ 1.25% $\pm$ 0.2% $\pm$ 1.0%
AVL 437c smoke meter	Smoke	0 to 100%	$\pm$ 0.1	$\pm$ 0.01
DP transmitter	EBP	–	$\pm$ 2kPa	$\pm$ 3%
EnginesoftLV 6.0	BTE BSFC	– –	– –	Derived Derived

$$U_{total} = \sqrt{\sum_{i=1}^{n}(u_i)^2} \quad (1)$$

$$= \sqrt{(CP)^2 + (HRR)^2 + (ID)^2 + (CT)^2 + (NOx)^2 + (BP)^2 + (BSFC)^2 + (BTE)^2 + (HC)^2 + (CO)^2 + (PM)^2}$$

$$\sqrt{(0.25)^2 + (0.55)^2 + (0.3)^2 + (0.25)^2 + (1.45)^2 + (0.6)^2 + (1.3)^2 + (0.75)^2 + (0.2)^2 + (0.25)^2 + (0.57)^2}$$

$$= \pm 2.38$$

The total uncertainty of a calculated parameter was obtained using the root-sum-square (RSS) method, assuming the individual uncertainties are independent. The combined uncertainty is given by Equation (1). Where, U_{total} is the total combined uncertainty of the measured or calculated parameter (–), u_i is the uncertainty associated with the *i* measured variable (with its respective unit), and n is the number of independent variables contributing to the measurement. Table 5 illustrates the relative magnitude of uncertainty for each measurement, providing a comprehensive overview of the measurement accuracy across the different parameters.

Table 5. Measured parameters' uncertainty.

Parameter	Uncertainty
In-cylinder pressure	± 0.25
Heat release rate	± 0.55
Ignition delay	± 0.3
In-cylinder temperature	± 0.25
NOx	± 1.45
BP	± 0.6
BSFC	± 1.3
BTE	± 0.75
HC	± 0.2
CO	± 0.25
PM	± 0.57

For parameters derived from multiple measured quantities, such as BTE and BSFC, the total uncertainty was obtained by propagating the uncertainties of the contributing variables using Equation (1).

2.2. Experimental Procedure

Numerous different orifices comprised 304 stainless steel plates, each featuring holes with diameters initially measuring 32 mm, with subsequent sizes reduced by 5 mm increments. The orifices were installed strategically within the exhaust pipe, resulting in an increase in back pressure as the diameter of the orifice decreased. This configuration enabled the generation of EBPs over a broad spectrum, ranging from 5.4 to 73.5 kPa. However, the performance and emissions were recorded at specific pressure values of 15 kPa, 30 kPa, 45 kPa, and 60 kPa using by the Rosemount 3051S series DP transmitter. The pressure magnitudes referenced are derived from [12], [13], who reported that EBP in single cylinder compression ignition (CI) engines can become detrimental at approximately 40 mm Hg (~5.5 kPa).

In this study, the EBP experienced by the engine far exceeded this threshold. The adjustment of the CR was achieved by rotating the CR adjustment knob 45 degrees clockwise, with the CR indicator observed concurrently to confirm precise readings. Load adjustments were performed via the load controller knob located within the control panel box, with engine speed monitored through the EnginesoftLV 6.0 software on the computer, based on the revolution count.

During the experimental tests, three key parameters were systematically varied, namely, CR, engine load, and EBP. A total of four test cases were conducted, with the engine speed maintained constant at 1 500 rpm across all cases. For each case, the load was varied from 25 to 100%, the CR ratio was adjusted between 12 and 18, and the EBP

was incrementally increased from 15 to 60 kPa. The specific operating conditions for each test case are detailed in Table 6. Within each test case, only the engine load and speed remained constant, while the CR and EBP were methodically varied. In the first case, tests began by varying all EBPs from 15 to 60kPa at the initial CR of 12, and this process was repeated for subsequent CRs values of 14, 16, and 18, with data collected at each step.

Table 6. Experimental test matrix.

Case	Speed (rpm)	Load (%)	CR	EBP (kPa)
1	1 500	25	12	15, 30, 45, 60
	1 500	25	14	15, 30, 45, 60
	1 500	25	16	15, 30, 45, 60
	1 500	25	18	15, 30, 45, 60
2	1 500	50	12	15, 30, 45, 60
	1 500	50	14	15, 30, 45, 60
	1 500	50	16	15, 30, 45, 60
	1 500	50	18	15, 30, 45, 60
3	1 500	75	12	15, 30, 45, 60
	1 500	75	14	15, 30, 45, 60
	1 500	75	16	15, 30, 45, 60
	1 500	75	18	15, 30, 45, 60
4	1 500	100	12	15, 30, 45, 60
	1 500	100	14	15, 30, 45, 60
	1 500	100	16	15, 30, 45, 60
	1 500	100	18	15, 30, 45, 60

The same systematic approach was applied to the remaining cases (2, 3, and 4). In these cases, engine speed showed minimal variation due to engine loading and was therefore considered constant at 1,500 rpm throughout the testing. However, the load was increased sequentially to 50%, 75%, and 100%. During these cases, the CR and EBP were again carefully varied to assess their effects comprehensively. For each of these test scenarios, detailed combustion analysis was performed, and performance parameters and emissions measurements were recorded. Combustion analysis and performance data were obtained using EnginesoftLV 6.0 software, while emissions were measured outside the exhaust pipe by means of a Combined PUC gas analyzer and AVL 437c smoke meter, as illustrated in Figure 2.

The adopted methodology follows a multifactorial experimental design. This approach is particularly suited to identifying cause-and-effect relationships between the independent variables (in this case CR, EBP, and engine load) and their effects. These effects include engine combustion, performance, and emissions [26],[27]. This allows for systematic investigation and statistically sound conclusions within the controlled environment of the test rig. This comprehensive experimental approach enabled an in-depth investigation of the combined effects of CR and engine load, revealing their influence on engine behavior under fluctuating EBP conditions.

2.2.1. Performance and combustion analysis

Combustion analysis was carried out using in-cylinder pressure data acquired as a function of crank angle. The apparent HRR was calculated using the first-law analysis for an open system, expressed by Equation (2):

$$\frac{dQ}{d\theta} = P\frac{\gamma}{\gamma-1}\left(\frac{dV}{d\theta}\right) + \frac{1}{\gamma-1}V\frac{dP}{d\theta} \quad (2)$$

Where $\frac{dQ}{d\theta}$ represented the HRR (J/°CA), γ represented the specific heat ratio, V was the in-cylinder volume (m^3), P was the in-cylinder pressure (bar), and θ was the crank angle (°CA).

In the present study, a constant value of $\gamma = 1.35$ was assumed. This value is commonly adopted for diesel combustion analysis and provides reliable comparative trends under varying operating conditions. The HRR was subsequently integrated with respect to crank angle to determine cumulative heat release. Combustion parameters such as ignition delay, combustion duration,

peak cylinder pressure, and crank angle locations of maximum pressure and HRR were derived from the processed pressure data. Performance parameters including BTE, BSFC, and indicated mean effective pressure (IMEP) were also computed using standard thermodynamic relations within the EnginesoftLV 6.0 software.

2.2.2. Fuel injection control

During all experimental tests, the fuel injection system settings were kept constant to ensure a consistent energy input and to isolate the effects of CR, EBP, and engine load. The fuel injection timing was maintained at the manufacturer's standard setting, and no adjustments were made throughout the testing campaign. Fuel quantity was governed by the mechanical fuel injection system inherent to the Kirloskar engine and varied only as a function of engine load, as per normal engine operation. No changes were introduced to injection pressure, nozzle geometry, or injection duration during the experiments. This approach ensured that variations in combustion, performance, and emissions could be attributed primarily to changes in CR, EBP, and load, rather than fluctuations in fuel delivery characteristic.

3. Results and Discussion

In diesel engines, various factors influence combustion efficiency. These include fuel quality, CR, load conditions, EBP, combustion chamber design, cetane number, fuel evaporation rate, injection timing, and pressure [28], [29]. Thus, improving these parameters usually results in better combustion, which in turn reduces fuel consumption, increases power output, and minimizes the emission of pollutants produced during the process. Overall, combustion efficiency is a key characteristic that significantly impacts both the performance and emissions of diesel engines.

3.1. Combustion analysis

This section investigates the effects of the combined operational parameters of the diesel engine, specifically CR, load, and EBP, under a constant engine speed of 1 500 rpm. The primary objective is to analyze the influence of EBP on the combustion process. This is done by examining key combustion characteristics, including in-cylinder pressure, heat release rate, and ignition delay, across varying operational conditions (CR and load).

3.1.1. Variation of in-cylinder pressure and HRR

Figures 3 to 6 illustrate the in-cylinder pressure and HRR responses under varying CR and EBP across different loads (25%, 50%, 75%, and 100%). EBP showed a complex influence on combustion, with its effects on HRR highly dependent on both CR and load. Increasing CR from 12 to 16 consistently raised both peak in-cylinder pressure and peak HRR across all load conditions, with the magnitude of improvement notable at higher loads. For example, at 25% load with an EBP of 15 kPa (Figure 3), the peak pressure rose from approximately 64 bar at CR = 12 to 69 bar at CR = 16, representing a 7.2% increase. Moreover, at 100% load under the same EBP (Figure 6), the peak pressure increased from 73 bar at CR = 12 to roughly 75 bar at CR = 14, a 2.7% increase.

The data further show that at high load (100%) and CR of 18, the engine did not achieve optimal performance when EBP reached a maximum of 60 kPa. This is likely because higher loads demand more fuel injection and energy release during combustion [30], [31]. Increasing CR from 12 to 16 increased the in-cylinder temperatures, pressures, and HRR, but an optimal balance appeared at medium to high loads (50% to 75%) with CRs of 14 to 16, where the effects of high EBP were moderately mitigated. Notably, at the highest EBP (60 kPa), peak in-cylinder pressures were most favourable at 75% load with CR = 16 (Figure 5c) and at 100% load with CR = 14 (Figure 6b). The HRR segment in Figures 3 to 6 depict the rate and amount of energy that could be transformed into beneficial work during the combustion process. It was mostly influenced by engine operating conditions (speed, load, CR, and EBP). Moreover, the ignition delay period greatly influenced this parameter.

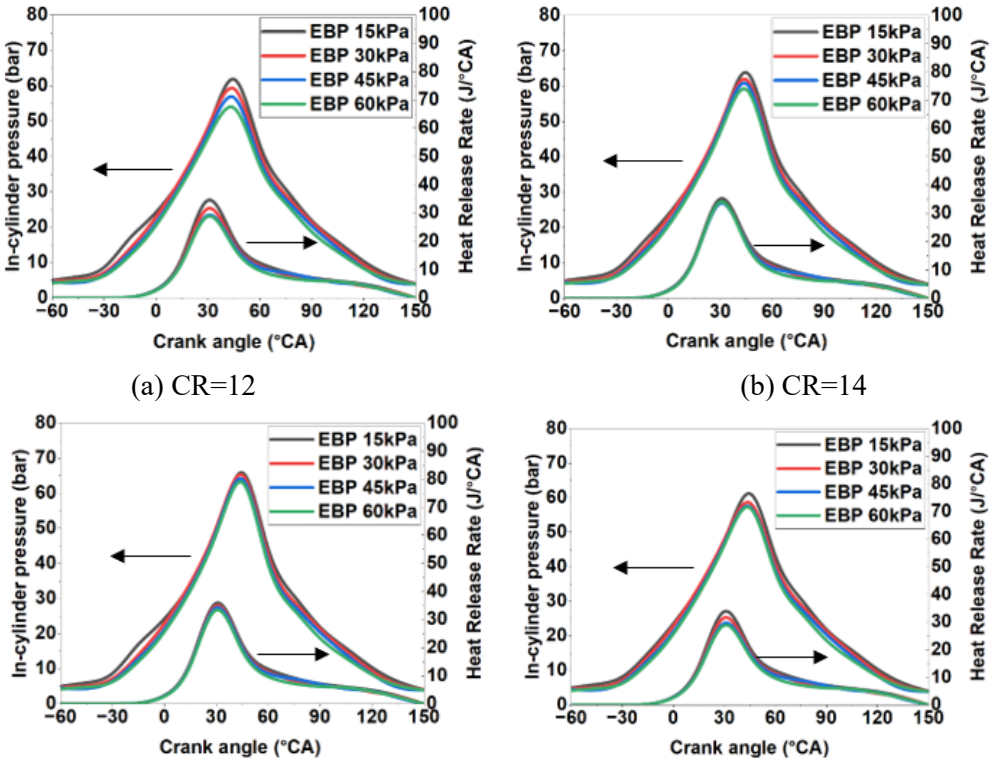

(a) CR=12 (b) CR=14

(c) CR=16 (d) CR=18

Figure 3. The variation of in-cylinder pressure and HRR at 25% load.

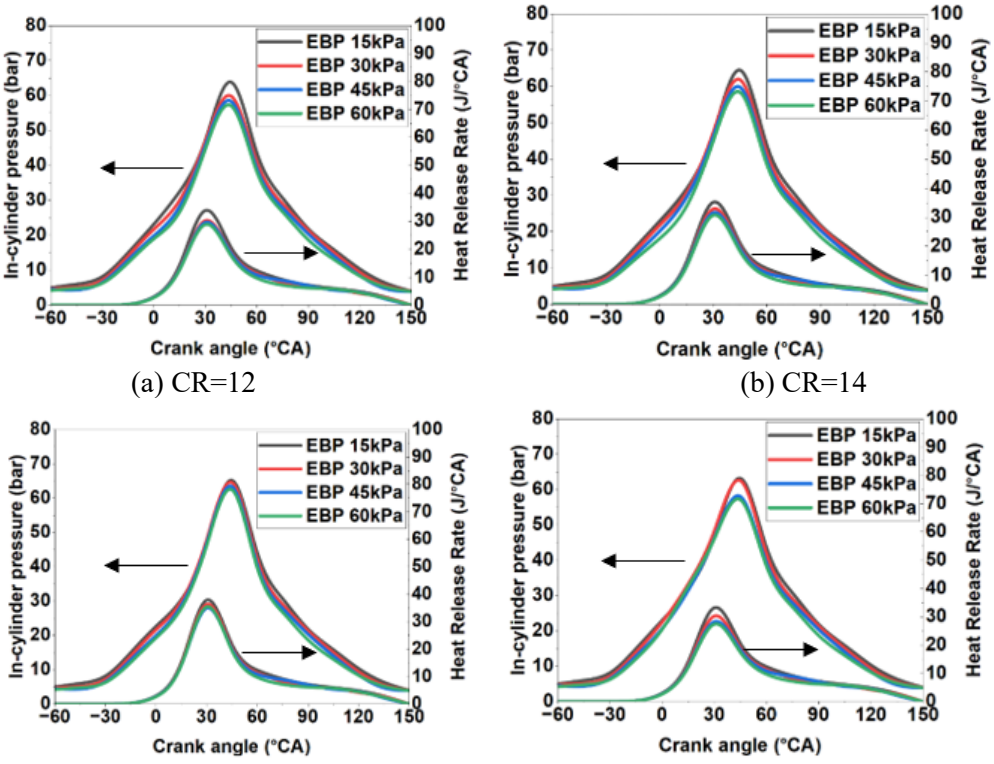

(a) CR=12 (b) CR=14

(c) CR=16 (d) CR=18

Figure 4. The variation of in-cylinder pressure and HRR at 50% load.

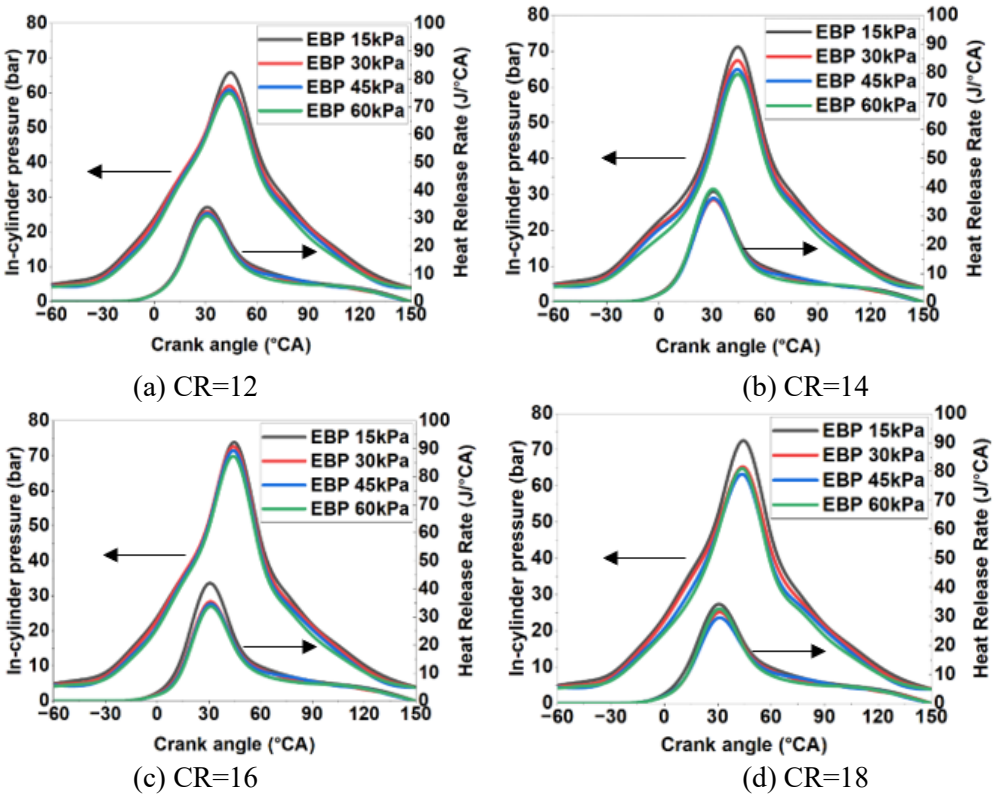

(a) CR=12 (b) CR=14

(c) CR=16 (d) CR=18

Figure 5. The variation of in-cylinder pressure and HRR at 75% load.

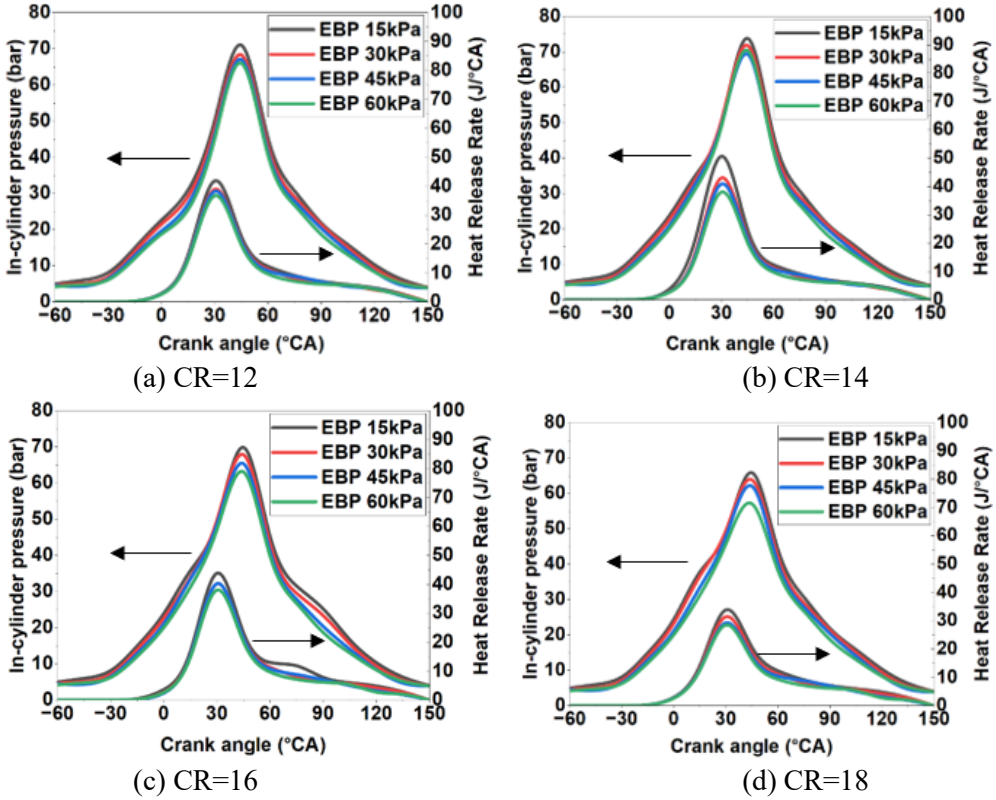

(a) CR=12 (b) CR=14

(c) CR=16 (d) CR=18

Figure 6. The variation of in-cylinder pressure and HRR at 100% load.

A key observation across the test cases is that increasing load and CR generally mitigates the adverse effects of EBP on HRR. For instance, a notable peak HRR of 40 J/°CA under maximum EBP of 60 kPa was observed at 75% load and CR of 14 as illustrated in Figure (5b). In contrast, at the same EBP but with a CR of 18, a slight decrease in peak HRR was consistently observed across all load conditions. This trend is likely due to the increase in-cylinder temperatures which enhances heat transfer during combustion [32]. Such heat transfer is influenced by increased residual exhaust gases and higher gas temperatures, potentially leading to uncontrolled combustion that can damage engine components. Additionally, the presence of trapped residual gases dilutes the fresh charge, reducing the effective air-fuel ratio [32], [33]. Lower HRR at higher CRs may have potentially resulted from compromised air-fuel mixing caused by high EBP and the effects of air entrainment [33]. Ultimately, these observations underscore the critical importance of balancing load and CR. This balance is necessary to effectively mitigate the effects of EBP and promote diesel engine combustion performance.

3.1.2. Influence of ignition delay

The effect of EBP under variation of load and CR shows a non-linear correlation. Figure 7 and Figure 8 illustrate this relationship in detail. They show how EBP influences the ignition delay period, measured in crank angle degrees, across different loads and CRs. Figure 7 indicates that the ignition delay decreased as the load increased from approximately 25% to 100%. This reduction was more noticeable under low to medium EBP conditions, ranging from 15 to 45 kPa. At a 25% load, the ignition delay ranged between 20 °CA and 24 °CA. As the load increased, the ignition delay dropped significantly. It reached a minimum of 12 °CA at full load (100%) with a medium EBP of 30 kPa.

When EBP increased further to 60 kPa, the ignition delay increased again. However, the continued increase in load partially reduced this negative effect. The ignition delay slightly decreased to about 16 °CA. A similar trend appeared when evaluating EBP under varying CRs. The main difference was the maximum ignition delay value. The highest ignition delay was 25 °CA, recorded at a CR of 12 and an EBP of 60 kPa. In contrast, the shortest ignition delay was 14 °CA. This occurred at a CR of 18 with EBP levels of 30 and 45 kPa.

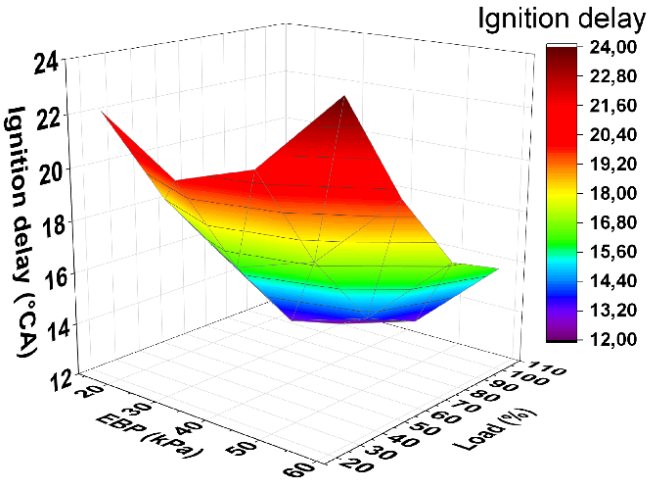

Figure 7. The influence of EBP on the ignition delay with individual variation of load.

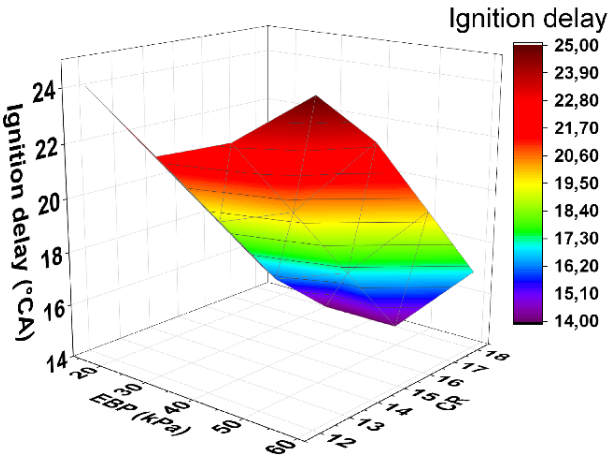

Figure 8. The influence of EBP on the ignition delay with individual variation of CR.

Figure 9 presents a 3D scatter plot that evaluates the influence of increasing EBP on ignition delay. The analysis also considers simultaneous variations in CR and load. The data show that ignition delay varied across all levels of EBP, load, and CR. For example, at EBP levels of 15 and 60 kPa, the ignition delay was higher at the start. This occurred when the load was 25% and the CR was 12. When the load increased to the range of 75%–100% and the CR increased to 16–18, the ignition delay became shorter. This indicates that increasing load and CR reduces the ignition delay period. The highest ignition delay observed was 23 °CA. This value is slightly lower than the highest delays recorded when the parameters were varied individually in Figure 7.

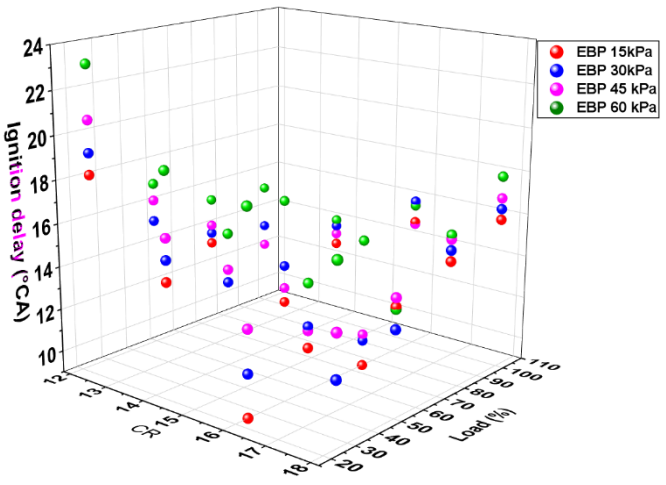

Figure 9. The influence of EBP on the ignition delay with simultaneous variation of CR and load.

In contrast, the shortest ignition delay was 10.5 °CA. This occurred at a CR of 16 and a load of 75%. The result shows that an optimal balance between load and CR can counteract the effects of EBP and shorten ignition delay. Therefore, both load and CR must be adjusted strategically. These findings also support the observations from Figures 3 to 6. Those figures showed that the highest load and highest CR do not always produce the best combustion performance. The analysis highlights the complex and sensitive behaviour of ignition delay. It also emphasizes the importance of controlling load and CR simultaneously to improve ignition delay under increasing EBP. Such control is essential for achieving optimal combustion performance.

To quantitatively describe the influence of load, CR, and EBP on ignition delay (ID), a modified Arrhenius-type correlation was employed. This approach is consistent with previous work by Ghareeb and Anjal [34] and Al-Shahrani [35]. In those studies, ignition delay is expressed as a function of pressure, temperature, and equivalence ratio, thereby forming a non-linear equation (Equation 3).

$$\tau_{id} = A\left(P_{ign}\right)^{-B}(\emptyset)^{-C}e^{\left(\frac{E_a}{RT_{ign}}\right)} \quad (3)$$

In this formulation, the ignition delay is influenced by the T_{ign}, $\emptyset$, P_{ign}, and empirical constants A, B, and C. The precise values of these constants are typically determined using the least squares fitting method. Equation (4) is obtained applying a logarithmic transformation to Equation (3):

$$\ln(\emptyset) = \ln(a) - B\ln\left(P_{ign}\right) - C\ln(\emptyset) + \frac{E_a}{RT_{ign}} \quad (4)$$

where, $\tau_{id,}$ is ignition delay in °CA, P_{ign} is ignition pressure in bar, $\emptyset$ is equivalence ratio, T_{ign} is ignition temperature in $°C$, E_a is the activation energy in kJ/mol, R is universal gas constant in kJ/kmol·$°C$ and A, B, C are empirical constants. To incorporate diesel engine condition parameters (load, CR, and EBP) into the ignition delay equations, their impact on the existing variables was carefully considered during the experimental work. These operational parameters do not directly appear in Equation (3) but influence τ indirectly through their effect on P, T, and φ.

a) Effect of Load

Increased load increases injected fuel quantity, leading to:

- Increase in equivalence ratio (φ)
- Increase in in-cylinder temperature (T)

These relationships were empirically approximated as:

$$\phi = a_1 + b_1\, Load$$
$$T = a_2 + b_2\, Load$$

Where Load is expressed as percentage (%).

b) Effect of Compression Ratio

Compression ratio primarily influences:

- In-cylinder temperature at the end of compression
- In-cylinder pressure

These were approximated as:

$$T = a_3\, CR^n$$
$$P = a_4\, CR^m$$

Where n and m are experimentally determined exponents.

(c) Effect of Exhaust Back Pressure

Increased EBP increases RGF, leading to:

- Increased initial charge temperature
- Reduced oxygen availability

These effects were represented as:

$$T = a_5 + b_5\, EBP$$
$$\phi = a_6 + b_6\, EBP$$

Where EBP is in kPa.

Substituting the above relations into Equation (3) gives the final ignition delay model:

$$\tau = a[P(cr)]^{-a}[\phi(load, ebp)]^{c}\exp\left(\frac{E_a}{R\,T(load, cr, ebp)}\right) \quad (5)$$

The functions a and b represent empirical dependencies between Ø, P_{ign}, T_{ign} and operational conditions. These varies based on the type of diesel engine and fuel being used and are determined experimentally.

The modified Arrhenius model presented in this study is conceptual and was used to explain the observed ignition delay trends. The empirical constants were not calibrated due to limited thermodynamic state measurements. Therefore, the model should be interpreted as a mechanistic representation rather than a predictive correlation.

3.1.3. Optimum in-cylinder temperature for reducing NOx

The relationship between NOx emissions and in-cylinder temperature is critical for understanding combustion efficiency, as it explores a fundamental trade-off in engine operation. High in-cylinder temperatures enable complete fuel oxidation, thereby enhancing combustion efficiency, yet they also promote the formation of NOx, a major pollutant [36]. This section investigated the optimal operating conditions for mitigating NOx formation under high in-cylinder temperatures. The tests focused on higher CRs (16 and 18) and loads (75% and 100%), as NOx formation is most prominent under these conditions.

Figures 10 to 13 illustrate the influence of in-cylinder temperature on NOx emissions across different operating parameters. The data consistently show that NOx formation increases with rising in-cylinder temperature, aligning with the Zeldovich mechanism, which hypothesizes that higher temperatures promote NOx formation [37]. The results indicate a clear trend; NOx emissions increase with higher EBP, with the highest levels observed at EBP of 60 kPa relative to lower EBPs across all tested conditions. Furthermore, increasing engine load from 75% to 100% results in increased NOx emissions, with levels rising from approximately 880 to 980 ppm at comparable in-cylinder temperatures and EBP conditions. Varying CR from 16 to 18 demonstrated a more pronounced impact: the CR of 18 revealed higher NOx compared to CR 16. Based on Figures 12 and 13, at an EBP of 60 kPa, NOx concentrations increased from 910 ppm at CR 16 to 1 170 ppm at CR 18. This indicates that although an increase in CR offers several advantages, it also presents certain drawbacks, notably the high formation of NOx emissions. Thus, a balance within engine operating conditions is essential.

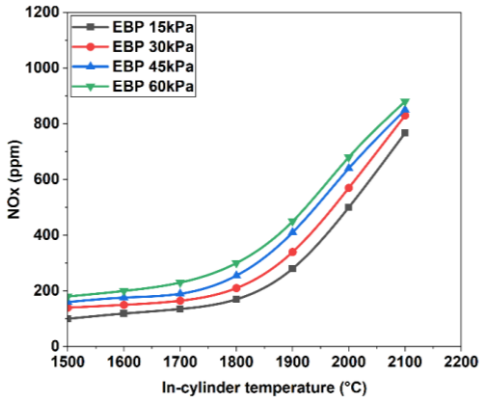

Figure 10. The influence of in-cylinder temperature on NOx Formation at varying EBP and 75% load.

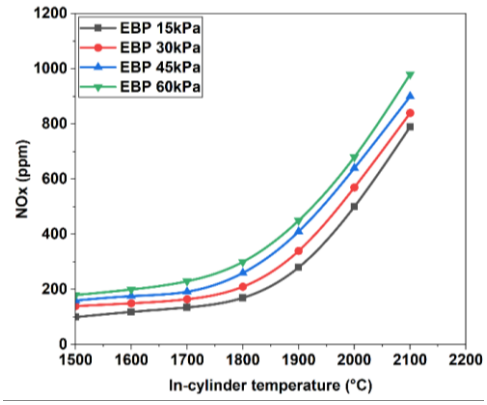

Figure 11. The influence of in-cylinder temperature on NOx Formation at varying EBP and 100% load.

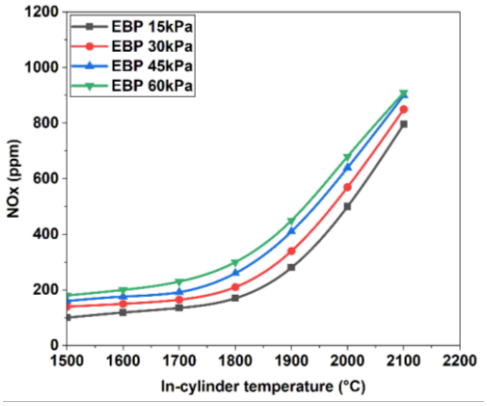

Figure 12. The influence of in-cylinder temperature on NOx Formation at varying EBP and CR=16.

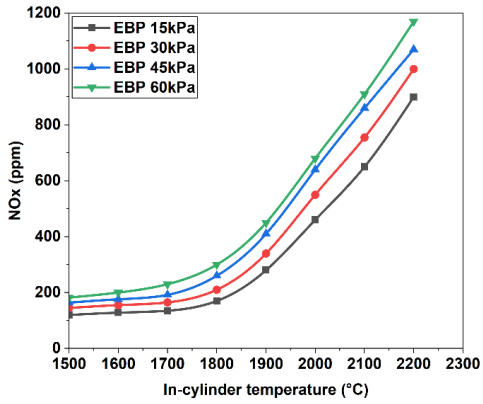

Figure 13. The influence of in-cylinder temperature on NOx Formation at varying EBP and CR = 18.

The effect of EBP on NOx formation, as shown in Figures 10 and 12, appeared nearly uniform at both 45 and 60 kPa. This suggests that higher EBP does not necessarily lead to increased NOx emissions. This phenomenon is attributed to the increased RGF associated with higher EBP, which influences combustion temperatures and thereby reduces NOx formation [38]. However, this relationship is modulated by other operating parameters such as engine speed, load and CR.

Ultimately, the findings indicate that the optimal operating conditions for mitigating NOx emissions occur at a load of 75% and a CR of 16. This represents a balanced compromise between combustion efficiency and pollutant formation. These observations substantiate the results discussed in Sections 3.1.1 and 3.1.2, where maximum combustion efficiency was achieved under the same parameters.

3.2. Performance characteristics

3.2.1. Influence of combined operating parameters

Figure 14 shows how BTE increases as the load rises from 25% to 75%. This trend is consistent across all four CRs, indicating that both CR and load contribute to improving BTE under increasing EBP. The increase in BTE is more pronounced at higher loads (from 25% to 75%), suggesting an interaction where both parameters enhance engine efficiency. Notably, this improvement is most evident at lower EBPs of 15 and 30 kPa, where the maximum BTE reached approximately 33% at 75% load and with a CR of 18. This suggests that, under these conditions, enhanced combustion efficiency and reduced losses occur due to higher CRs. Higher CRs increase peak cylinder pressures and temperatures, promote more complete combustion and greater gas expansion, and ultimately improve work output [39].

At higher loads and EBP of 60 kPa, BTE reduced sharply, reaching as low as 17% at 100% load and a CR of 18. This represents the lowest BTE observed across all operating conditions. Contrary to the discussion above, excessively high temperatures under maximum loads and CRs can result in increased heat transfer to the cooling system and engine components. This may reduce the heat available for useful work. Additionally, excessive load may cause incomplete combustion, influenced by factors such as limited air-fuel mixing, longer fuel injection durations, and increased cylinder pressures [40]. These effects reduce the conversion efficiency of fuel energy into mechanical work, amplifying the reduction in BTE under these conditions.

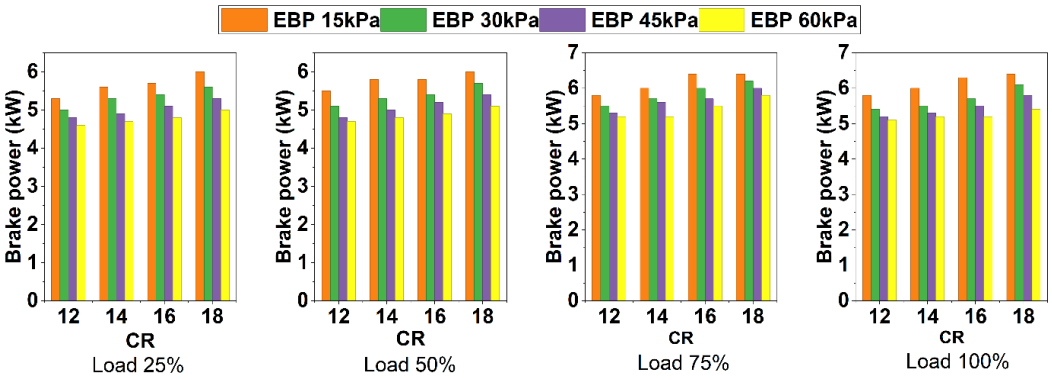

Figure 14. Effect of combined operating parameters on brake power

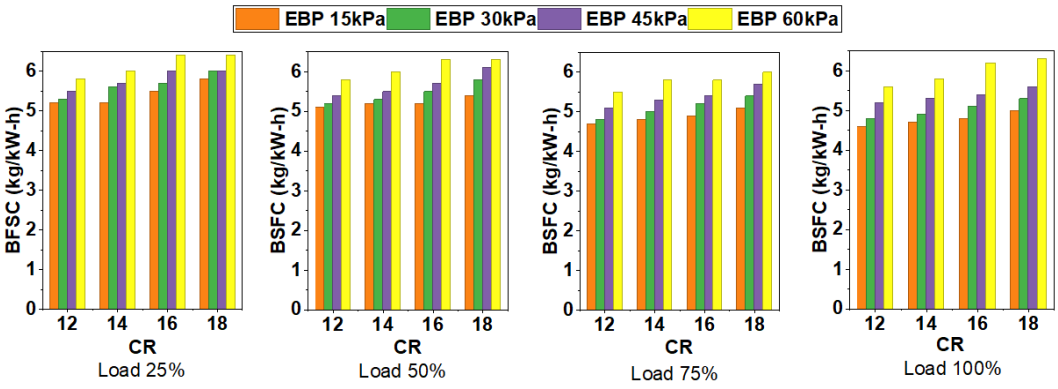

Figure 15. Effect of combined operating parameters on BSFC

Few studies demonstrated that although CR normally benefits the engine, these benefits are almost eliminated by the increase in EBP [25], [41]. However, Figure 15 shows that increasing CR led to an increase in brake power across all four conditions. The brake power increased from a minimum of 4.7 kW at 25% load, CR of 12, and EBP of 60 kPa to a maximum of 6.4 kW at 100% load, CR of 18, and EBP of 15 kPa. Since it has been proven that CR alone is not able to sustain the increase in EBP, the load had a greater influence on gradual increase in brake power. Moreover, some studies have shown that the load alone is also insufficient in sustaining high EBP conditions. This points towards the balance of these two operating conditions to overcome the negative influence posed by EBP in reducing the brake power.

Figure 15 shows that a high EBP of 60 kPa consistently increased the BSFC. Only small reductions were observed across different load conditions. This effect was especially noticeable at 100% load. The BSFC increased to 6.1 kg/kWh at a CR of 16 and 6.2 kg/kWh at a CR of 18. The higher BSFC at high EBP and high load can be linked to increased fuel demand required to meet power output. In addition, the benefits normally associated with higher load, such as improved combustion efficiency, did not increase proportionally. As a result, BSFC remained high.

The increase in BSFC at high CR suggests that higher cylinder pressure may create greater frictional losses. The pressure on the piston and cylinder walls likely reduces mechanical efficiency and increases fuel consumption [42]. However, at 75% load, the engine showed improved performance. The BSFC decreased to 5.5 kg/kWh at a CR of 12 and an EBP of 60 kPa. Overall, the results indicate that high CR and high load do not always produce optimal engine performance. Increasing EBP continued to negatively affect BSFC even when CR and load were increased. This confirms a non-linear and complex interaction when adjusting engine operating conditions to achieve better BSFC efficiency.

3.2.2. Influence of heat transfer

Heat transfer from the in-cylinder walls to the cooling system is a major challenge in improving engine performance. Some parameters, such as brake power, improve when load and CR increase. This happens because higher load and CR raise the in-cylinder temperature and the heat transfer rate. However, other parameters, such as BTE and BSFC, are directly affected by these operating conditions, as shown in Section 3.2.1. In IC engines transfer energy through three main paths: useful work, engine cooling through the coolant, and exhaust gases, as shown in Figure 16.

Figure 17(a) shows that these energy flows are roughly equal. Each account for about one-third of the energy released from fuel [43], [44], [45]. In some cases, useful mechanical work can be slightly higher, depending on engine operating conditions. Maintaining this balance is important for optimal engine performance.

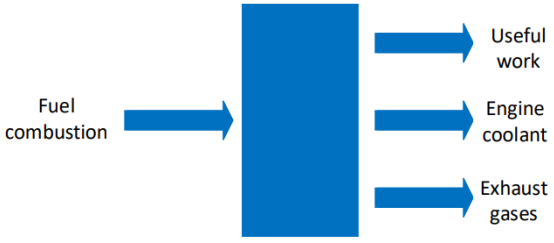

Figure 16. Heat distribution in an IC Engine.

When load and CR increase excessively, this balance is disturbed. As shown in Figure 17(b), useful work decreases while heat rejected to the cooling system increases. Excessive heat transfer may damage engine components and reduce overall efficiency. Therefore, predicting heat transfer factors such as heat flux, thermal loads, and gas-side parameters is necessary. The prediction should consider the maximum operating load, CR, and EBP of the engine.

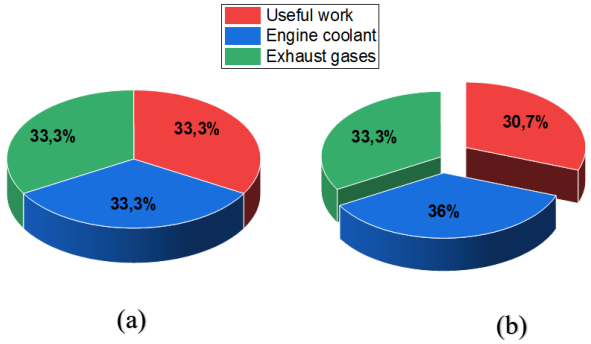

Figure 17. Common heat distribution (a) compared to typically distrusted system due to excessive load and CR (b).

The lack of detailed mathematical models describing the actual mechanisms governing heat transfer between combustion gases and cylinder walls, primarily caused by the high temperatures resulting from the simultaneous increase in CR, load, and EBP makes these predictions challenging. Although it is known that the exceptionally high heat fluxes are driven by strong temperature gradients within the boundary layer, predicting these values remains complex. However, based on recent advancements [46], [47], the following equations can be employed to estimate the heat flux, assuming that heat transfer is purely conductive (Equation 6).

$$\left.\frac{Q}{A}\right|_y = -k\left.\frac{\delta T}{\delta y}\right|_{y=0+} \tag{6}$$

Since the boundary conditions correspond to heat transfer described by Newton's law between the surface at temperature T_w and the fluid at temperature T_g. Therefore, the mean heat transfer coefficient can be expressed as Equation 7:

$$h(T_g - T_w) = -k\left.\frac{\delta T}{\delta y}\right|_{y=0+} \tag{7}$$

If the gradient is approximated as linear through the boundary layer, a connection between the heat transfer coefficient and the thermal conductivity of the gas mixture inside the boundary layer can be established using the relation expressed in Equation 8:

$$h = \frac{k}{\delta_t} \tag{8}$$

where Q is the heat transfer rate, A is the piston area, k is the thermal conductivity which depends on the cylinder wall material, h is the heat transfer coefficient, T_g is the gas mixture temperature, T_w is the cylinder wall temperature, and δ_t is the thermal boundary layer thickness.

By applying Equations (6) and (7), a conductive heat flux can be estimated. Ultimately, future designs could focus on the piston and cylinder dimensions based on the heat flux predicted at maximum CR, load, and EBP. These are conditions in which excessive heat generation occurs. Additionally, the thermal conductivity values could assist in selecting appropriate cylinder materials. Other recent advancements have demonstrated that improving heat transfer in IC engines requires integrating both conduction and convection methods [45], [47]. This approach is acceptable since the engine's heat transfer process follows the analogy illustrated in Figure 16.

Based on the analogy in Figure 18, heat transfer between the surfaces and the cooling system can be analyzed using the simple Newton's steady-state law. This is because both the surface and the cooling fluid can be assumed to be at constant temperatures. The resistances associated with the cylinder wall and the coolant are well defined. The complexity arises in evaluating the heat transfer coefficient between the gas and the walls, h_g. This is especially challenging under conditions of excessive in-cylinder temperatures caused by a maximum CR of 18, load of 100%, and EBP of 60 kPa. Clearly, this phenomenon is unsteady, and it is not guaranteed that all the heat dissipated from the gas mixture and walls is effectively transferred to the coolant.

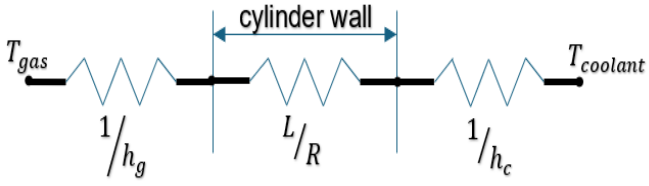

Figure 18. Heat transfer analogy for IC engines.

Recent advancements in predicting coolant thermal load under maximum engine operating conditions have been benchmarked by Sanli et al. [48]. This work has been further complemented by the contributions of Suzuki et al. [49] and Dabbaghi et al. [50], who have also recently employed the following approach (Equation 9):

$$Nu = aRE^m \tag{9}$$

where Prandtl number (Pr) has been omitted since it varies little in gases and its effects can be incorporated into the coefficient a. The Nusselt number (Nu) and Reynolds number (Re) are defined in Equations 10 and 11 as:

$$Nu = \frac{\dot{Q}B}{k_g A_p (T_g - T_c)} \tag{10}$$

$$Re = \frac{\dot{m}_g B}{\mu_g A_p} \tag{11}$$

where, $\dot{Q}$ is the heat transfer rate to the engine coolant, $\dot{m}_g$ is the charge mass flowrate, A_p is the piston area, B is the cylinder bore, T_g and represents a mean effective gas temperature for the engine cycle. The numerical values of T_g and corresponding k_g and μ_g are typically considered as functions of the overall fuel-air ratio. The factors *a* and m are selected to achieve the best agreement with experimental results. In this case this selection will be informed by the engine maximum operating conditions of a CR of 18, load of 100% and EBP of 60kPa. Once the a and m factors have been established based on the experimental data, Nu and Re are simplified and given by Equations (12) and (13):

$$Nu = \frac{h_e B}{k_g} \tag{12}$$

$$Re = \frac{GB}{\mu_g} \tag{13}$$

where Re is defined as a gas-side parameter, G is the gas mass rate of flow divided by A_p, and h_e which can be expressed by Equation (14):

$$h_e = \frac{\dot{Q}}{A_p (T_g - T_c)} \tag{14}$$

By integrating the above equations with all physical quantities expressed in consistent units, the following correlation for the overall heat flux was derived (Equation 15):

$$\frac{\dot{Q}}{A_p} = a \frac{k_g}{B} (T_g - T_c) \left(\frac{GB}{\mu_g}\right)^m \tag{15}$$

The above correlation can be used to predict gas-side engine heat transfer. It offers valuable insights into the factors that influence how heat is transferred from the hot combustion gases to the engine's internal surfaces, primarily the cylinder walls and piston. This prediction relies on known or estimable parameters such as the air-fuel ratio and mass flow rates. Furthermore, this approach provides guidance in establishing the empirical correlation for the overall heat transfer coefficient within the cooling system. The derivation employed can also be used to predict the engine coolant thermal load based on varying engine operating conditions such as loads, CRs and EBPs.

Based on the correlations and fundamental principles discussed above, additional steps were undertaken in this study to enable a rigorous quantification of in-cylinder heat loss. This was achieved using the Hohenberg correlation shown in Equation (16). This was followed by a more comprehensive thermodynamic analysis.

$$h = 130\, V^{-0.06} P^{0.8} \tag{16}$$

Where, h= heat transfer coefficient (W/m²·K), V= instantaneous cylinder volume (m³), P= in-cylinder pressure (MPa), T= in-cylinder gas temperature (K). The instantaneous heat flux is given by:

$$q'' = h(T_g - T_w) \tag{17}$$

And total in-cylinder heat loss rate can be expressed as:

$$\dot{Q} = hA(T_g - T_w) \tag{18}$$

To strengthen the heat loss analysis under varying CR and EBP conditions, the following three operating cases shown in Table 7 were quantified. It should be noted that engine load influences heat transfer indirectly, through its effect on peak pressure and temperature; therefore, it was not explicitly included in the test cases below. The three test cases are summarized in Table 8 for convenient comparison. Moreover, the reinforced thermal interpretation is presented in Table 9.

Table 7. Three test cases.

Case	CR	EBP (kPa)	Peak Pressure (MPa)	Peak Temp (°C)
1	12	30	6.5	1727
2	18	30	7.0	1877
3	18	60	7.5	1977

Table 8. Summary of the three test cases.

Case	CR	EBP (kPa)	Heat Transfer Coefficient, h(W/m²·K)	Heat Flux, q''(kW/m²)	Total Heat Loss, $\dot{Q}$(kW)	Increase vs Case 1 (%)
1	12	30	520	806	25.8	-
2	18	30	563	963	30.8	19.4
3	18	60	593	1071	34.3	32.9

Table 9. Reinforced heat loss analysis summary.

Thematic Area	Operating Change	Thermodynamic Effects	Heat Transfer Consequence	Quantified Impact	Overall Implication
Thermal penalty of high CR	Increase in CR	↑ Peak pressure ↑ Peak temperature ↑ Convective heat transfer coefficient (h)	Stronger gas-to-wall temperature gradient and enhanced convection	~12–13% increase in instantaneous wall heat loss	Improved combustion but significantly higher thermal loading on piston and liner
Effect of EBP	Increase in EBP	↑ RGF ↑ In-cylinder temperature Slight ↑ Pressure	Further increase in heat transfer coefficient and wall heat flux	Additional ~13% increase in heat flux beyond CR effect	Amplifies thermal stress under high-load conditions
Combined High CR + High EBP	Maximum CR and EBP	Highest combustion intensity and peak thermodynamic states	Maximum wall heat rejection	~25% increase in total heat loss compared to baseline ≈30% of fuel energy rejected to walls	Significant thermal penalty despite improved combustion phasing
Combustion efficiency trade-off	Simultaneous high CR and EBP	Shorter ignition delay More intense combustion	Increased conductive and convective heat losses	Net reduction in BTE at extreme settings	Demonstrates clear thermodynamic trade-off between combustion improvement and heat rejection

Case 1: CR 12, 30 kPa EBP

$$h_1 = 130(5.29 \times 10^{-5})^{-0.06}(6.5)^{0.8}(2000)^{-0.4}$$
$$h_1 \approx 520\, W/m^2 \cdot K$$

Heat flux:

$$q_1'' = 520(2000 - 450)$$
$$q_1'' \approx 806{,}000\, W/m^2 = 806\, kW/m^2$$

Total heat loss:

$$\dot{Q}_1 = 520 \times 0.032 \times 1550$$
$$\dot{Q}_1 \approx 25.8\, kW$$

The reinforced heat loss analysis clearly demonstrates that increasing CR and EBP, while beneficial for combustion intensity and ignition characteristics, results in a measurable thermal penalty. The combined high CR and high EBP condition produced approximately a 25–33% increase in total wall heat rejection relative to the baseline case. This indicates that nearly one-third of the supplied fuel energy may be rejected to the combustion chamber walls under extreme operating conditions. Although a higher CR improves thermal efficiency in principle, the amplified convective heat transfer under high-pressure and high-temperature conditions can counteract these gains. This is achieved by increasing conductive and convective losses. The results therefore highlight a critical thermodynamic trade-off: improvements in combustion phasing and intensity must be balanced against increased thermal loading and heat rejection to avoid reductions in BTE and excessive component stress.

3.3. Emission analysis

The analysis presented in Figure 19 reveals a general trend whereby EBP is associated with a slight increase in CO emissions. Specifically, at a 25% load and a CR of 12, there is an observed difference of approximately 15 ppm in CO emissions between an EBP of 15 and 60 kPa, representing a 13% increase. This indicates that increasing EBP tends to marginally increase CO emissions under these conditions. From a combustion perspective, CO formation is strongly influenced by the HRR and the phasing of combustion. Conditions that delay complete oxidation, such as retarded combustion phasing (later CA50) or reduced peak temperatures, can promote incomplete combustion and consequently increase CO levels [42].

At a 50% load, a clear reduction in CO emissions is observed across all CRs. This suggests that load has a stronger influence on CO formation than CR. The result agrees with the understanding that higher load increases combustion temperature and pressure. Higher temperature improves combustion efficiency. Improved combustion phasing under these conditions shortens the oxidation duration. This reduces incomplete combustion products. However, excessively high temperatures or locally rich zones may still promote CO formation if oxygen is insufficient for complete combustion [48].

When the load increases further to 75% and 100%, CO emissions rise again. The highest values occur at full load. This behaviour is likely caused by poor air–fuel mixture conditions that cannot satisfy the high fuel demand at maximum load. The result is incomplete combustion and increased CO formation. In addition, a shortened ignition delay and rapid diffusion combustion may limit full oxidation of partially oxidized fuel compounds. Overall, the results show that engine load has a stronger effect on CO emissions than CR. They also highlight the need for optimized combustion phasing and proper air–fuel conditions, especially at high load, to reduce CO formation.

Figure 19 shows that HC emissions increased significantly at low (25%) and high (100%) engine loads. Peak values reached 300 ppm and 270 ppm at the maximum EBP of 60 kPa. This behaviour is linked to the effect of engine load on in-cylinder temperature and combustion development. At higher loads, higher combustion temperature normally improves HC oxidation. It also reduces incomplete combustion caused by cold cylinder walls [34]. However, excessively high EBP counteracts these benefits. It likely alters combustion phasing and modifies the heat release rate, which increases HC emissions. Similar observations were reported in earlier studies [36], [38].

Across all conditions, an EBP of 60 kPa consistently produced the highest HC emissions. This indicates that such EBP levels are unsuitable for clean combustion even when CR is increased. In contrast, HC emissions were lowest at intermediate loads of 50–75%. This occurred especially with lower to medium CR values (CR 12–16). This suggests an optimal balance between ignition delay, premixed combustion intensity, and heat release behavior. The results confirm a complex, non-linear interaction between engine load, CR, EBP, and combustion phasing. Therefore, advanced combustion control strategies are necessary. These include homogeneous charge compression ignition (HCCI), precise injection timing, improved injection patterns, and advanced fuel delivery systems. One example is common rail injection, which helps reduce emissions under varying engine conditions.

Figure 21 illustrates the variation in smoke opacity as a function of the combined engine operating parameters. The general trend indicates that smoke opacity decreases with increasing load and CR up to 75% load. This reduction can potentially be attributed to improved combustion efficiency resulting from the combined effects of increased load and CR. These factors enhance in-cylinder pressure and temperature, thereby promoting more complete fuel oxidation and reducing the formation of smoke and particulate matter (PM). Considering combustion characteristics, optimized ignition delay and controlled HRR during the premixed phase promote better air–fuel mixing and mitigate soot formation. It is worth noting that in diesel engines visible smoke typically begins to form when smoke opacity exceeds 5% [33]. As shown in Figure 21, only four test conditions exceeded this threshold, specifically at 25 and 100% loads with CRs of 12 and 14, all at EBP of 60 kPa

These findings suggest that excessive EBP can reduce some of the benefits gained from increasing load and CR. This happens when in-cylinder temperatures and combustion phasing become unfavourable. At low load, temperatures may be too low to sustain complete

combustion. At full load, advanced combustion phasing (earlier CA50) and increased premixed HRR can raise local combustion temperatures and increase NOx formation. High NOx emissions are commonly linked to advanced combustion phasing and high peak temperatures. In addition, a long ignition delay strengthens the premixed combustion phase. This increases HRR and in-cylinder temperature, which promotes thermal NOx formation.

On the other hand, overly delayed combustion increases CO and HC emissions because oxidation becomes incomplete. These results emphasize the importance of precise injection timing and combustion phasing control in IC engines. Emissions are strongly governed by HRR behaviour, ignition delay, and peak combustion temperature. Therefore, injection timing must be adjusted according to specific combinations of load, CR, and EBP. Proper adjustment helps minimize smoke formation, control NOx production, and improve overall engine performance.

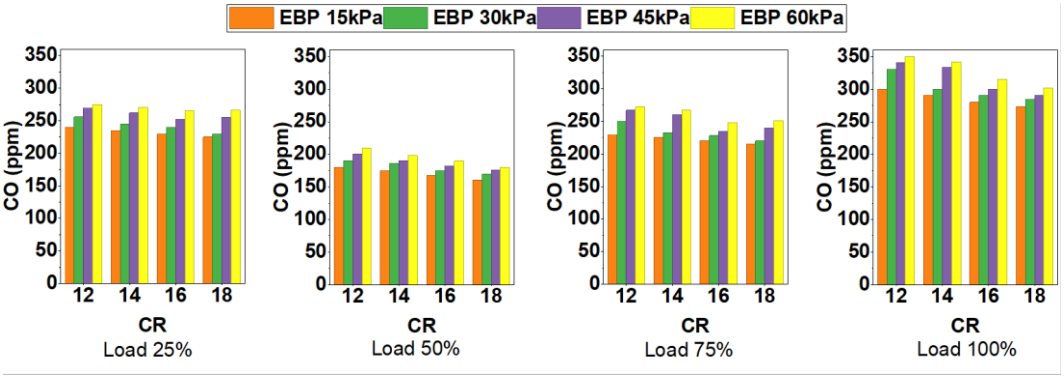

Figure 19. Effect of combined operating parameters on CO.

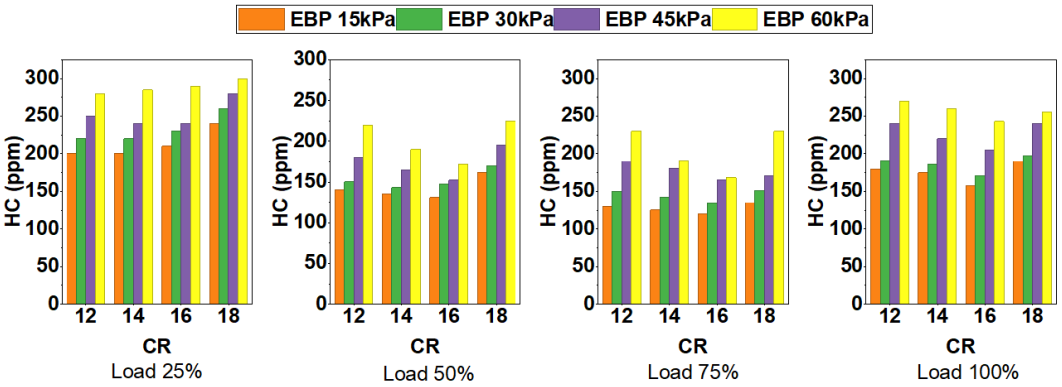

Figure 20. Effect of combined operating parameters on HC.

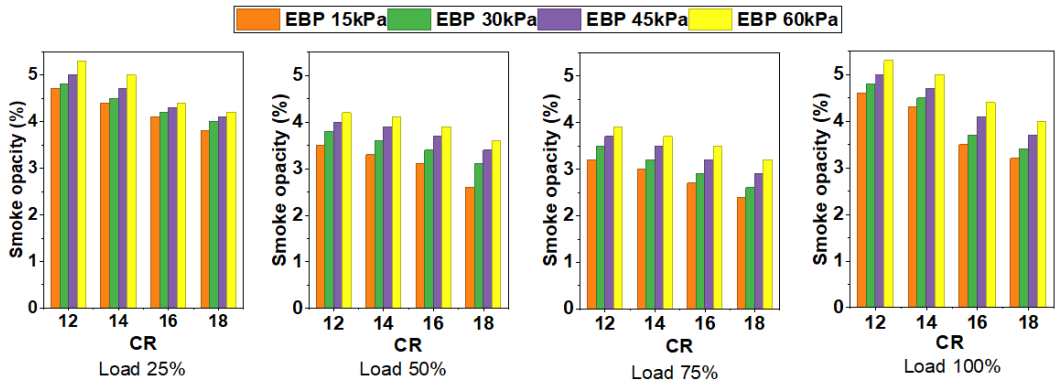

Figure 21. Effect of combined operating parameters on smoke opacity.

4. Conclusion and Further Studies

This experimental study comprehensively investigated the combined effects of CR, load, and EBP on diesel engine combustion, performance, heat transfer, and emission characteristics. The experiments were conducted at a constant engine speed of 1 500 rpm. Key combustion parameters, including in-cylinder pressure, HRR, and ignition delay, were analysed. In addition, BTE, BSFC, and emissions such as NOX, CO, HC, and smoke opacity were evaluated. The following conclusions are drawn from the experimental study:

- Increasing CR (12 to 16) and moderate-to-high loads (50% to 75%) improved in-cylinder pressure, HRR, and combustion efficiency. However, excessive CR (18) and EBP (60 kPa) increased in-cylinder temperatures and residual gases, which reduced HRR and compromised combustion efficiency. Ignition delay generally shortened with higher CR and load but was extended under maximum EBP (60 kPa). Optimal ignition timing was observed at CR = 16 and 75% load, confirming that balanced operating parameters are more effective than extreme conditions.
- BTE peaked at approximately 33% under moderate loads (50 to 75%) and low EBP (15 to 30 kPa). In contrast, it decreased significantly at high CR and load with 60 kPa EBP, resulting in an increase in BSFC.Brake power improved with CR and load but could not fully make up for the losses that are due to excessive EBP.
- Higher CR and load resulted in high heat flux and cooling requirements, reducing network output. Predictive heat transfer models (Nu–Re correlations) are essential for piston and cylinder design under maximum operating conditions.
- CO and HC were minimized at 50% to 75% load and CR = 12 to 16. By comparison, NOx emissions increased as CR and load increased, necessitating careful in-cylinder temperature management. Smoke opacity followed a similar trend, with higher levels at a maximum EBP (60 kPa) and full load, validating the importance of maintaining moderate operating conditions.

Overall, the current research reveals that optimum diesel engine operation is achieved at CR = 14 to 16, 50 to 75% load, and EBP not exceeding 45 kPa. These findings highlight the importance of balanced engine conditions and the implementation of advanced control strategies. Future studies should investigate the effects of biodiesel blends and variations in engine speed to identify advancements that enable the use of higher CRs (18 to 22) and full load (100%). Such developments may serve as effective countermeasures against excessive EBP (60 kPa or more), thereby sustaining optimal engine performance.

Extending the study to include variable-speed operation and transient loading conditions would provide a more comprehensive understanding of combustion behavior, heat transfer, and emission characteristics. This approach would better reflect practical engine operating conditions. Other scholars should assess higher CRs (18 to 22) operation as possible strategies to counteract excessive EBP (60 kPa or higher), thereby maintaining optimal engine performance. Furthermore, effective heat management strategies should be developed and implemented to preserve performance. These measures would also help prevent potential component stress or damage associated with elevated EBP conditions.

Conflict of Interest

The authors declare that there are no conflicts of interest related to this work.

Data Availability Statement

All data supporting the findings of this study are included within the article. Additional information can be requested from the corresponding author.

Supporting Agencies

University of Kwa-Zulu Natal, South Africa.

Acknowledgements

The authors would like to acknowledge the valuable contributions of Prof. Inambao, who sadly passed away

before the submission of this manuscript. His input and support were instrumental to the development of this work, and the authors are grateful for his contribution.

References

[1] A. Sozhipillai, P. Kasi, R. Palani, and J. Govindaraj, "Optimisation of Diesel Spray, Combustion and Emission Characteristics of Biofuel by Varying Injection Pressure and Timing in a DICI Engine," *International Journal of Ambient Energy*, vol. 42, no. 14, pp. 1655–1668, 2021, doi: 10.1080/01430750.2019.1627402.

[2] P. Shanmughasundaram, and T. I. Manosh, "Emission Characteristics of Single Cylinder Diesel Engine Using Blends of Rubber Seed Biodiesel Using Taguchi Method," *Journal of Material and Environmental Sciences*, vol. 6, no. 6, pp. 1774-1779, 2015..

[3] P. Raghu, K. Thilagan, M. Thirumoorthy, Siddharth Lokachari, and N. Nallusamy, "Spray Characteristics of Diesel and Biodiesel in Direct Injection Diesel Engine,", vol. 768, 2019, doi: 10.4028/www.scientific.net/amr.768.173.

[4] V. S. Kumbhar, A. Shahare, and G. Awari, "Review on Reactivity Controlled Compression Ignition Engines: an Approach for BSVI emission Norms," *IOP Conference Series: Materials Science and Engineering*, vol. 1170, no. 1, p. 012011, Jun. 2021, doi: 10.1088/1757-899x/1170/1/012011.

[5] M. Puškár and P. Tarbajovský, "Complex analysis of combustion and emission parameters of bio-renewable fuel mixtures in dual-fuel mode," *Social Science Research Network*, vol. 16, no. 6, 2022, doi: 10.1002/bbb.2415.

[6] M. Mirmohammadsadeghi, "Investigation of diesel-ethanol and diesel-gasoline dual fuel combustion in a single cylinder optical diesel engine," Ph.D. dissertation, Dept. Mech. Eng., Eindhoven Univ. Technol., Eindhoven, Netherlands, 2018.

[7] W. Han, B. Li, S. Pan, Y. Lu, and X. Li, "Combined effect of inlet pressure, total cycle energy, and start of injection on low load reactivity controlled compression ignition combustion and emission characteristics in a multi-cylinder heavy-duty engine fueled with gasoline/diesel," *Energy*, vol. 165, pp. 846–858, 2018, doi: 10.1016/j.energy.2018.10.029.

[8] Zetai Ma et al., "Experimental study on influence of high exhaust backpressure on diesel engine performance via energy and exergy analysis," *Energy*, vol. 263, 2022, doi: 10.1016/j.energy.2022.125788.

[9] Abdulkarim Youssef, and Amr Ibrahim, "A numerical investigation on the effect of altering compression ratio, injection timing, and injection duration on the performance of a diesel engine fuelled with diesel-biodiesel-butanol blend," *Clean energy*, vol. 8, no. 9. 2024, doi: 10.1093/ce/zkae055.

[10] Christopher Selvam Damian and Yuvarajan Devarajan, "Performance and emission analysis of Sterculia foetida biodiesel enhanced with butanol: Combustion efficiency and emission mitigation," *Results in Engineering*, vol. 25, p. 104586, 2025, doi: 10.1016/j.rineng.2025.104586

[11] Sinnappadass Muniyappan, and Ravi Krishnaiah, "Optimizing engine operating parameters for enhanced performance in a combustion-enhanced ternary-fuelled compression ignition engine," *Scientific Reports*, vol. 15, no. 1, 2025, doi: 10.1038/s41598-025-05628-3.

[12] M. U. H. Joardder, M. S. Uddin, and M. M. Roy, "Effect of engine backpressure on the performance and emissions of a CI engine," in *Proceedings of the 9th International Conference on Mechanical Engineering (ICME 2011)*, S. M. Nazrul Islam, Ed. Dhaka, Bangladesh: Department of Mechanical Engineering, BUET, Dec. 2011, pp. 1-5.

[13] S. Desale, D. Patil, and R. R. Arakerimth. "Experimental analysis of engine exhaust back pressure on emission characteristics of four cylinder diesel engine." In *Int. Conf. Recent Advances in Mechanical Engineering in Collaboration with Int. J. Engineering and Management Research*, pp. 102-105. 2015.

[14] M. R. Ebrahimnataj, et al., "The effect of soot accumulation and backpressure of an integrated after-treatment system on diesel engine performance," *Journal of Thermal Analysis and Calorimetry*, vol. 147, no. 15, pp. 8943–8956, 2021, doi: 10.1007/s10973-021-11135-0.

[15] L. Huang, J. Liu, R. Liu, Y. Wang, and L. Liu, "Experimental investigation on combustion and performance of diesel engine under high exhaust back pressure," *Machines*, vol. 10, no. 10, p. 919, Oct. 2022, doi: 10.3390/machines10100919

[16] Y. Gülmez and G. Özmen, "Effects of exhaust backpressure increment on the performance and exhaust emissions of a single cylinder diesel engine," *Journal of ETA Maritime Science*, vol. 9, no. 3, pp. 177–191, Sept. 2021, doi: 10.4274/jems.2021.25582.

[17] R. R. Renish, A. J. Selvam, R. Čep, and M. Elangovan, "Performance, emission and combustion characteristics of a VCR engine fueled with sea mango biodiesel/diesel blends," *Processes*, vol. 10, no. 8, art. no. 1469, Jul. 2022, doi: 10.3390/pr10081469.

[18] R. C. Costa and J. R. Sodré, "Compression ratio effects on an ethanol/gasoline fuelled engine performance," *Applied Thermal Engineering*, vol. 31, no. 2–3, pp. 269–276, Jan. 2011, doi: 10.1016/j.applthermaleng.2010.09.007.

[19] A. A. Shaik, S. R. Reddy, V. D. Raju, and M. Govindarajan, "Combined influence of compression ratio and EGR on diverse characteristics of a research diesel engine fueled with waste mango seed biodiesel blend," *Energy Sources, Part A: Recovery, Utilization, and Environmental Effects*, vol. 42, no. 19, pp. 1–24, 2020, doi: 10.1080/15567036.2020.1811809.

[20] G. V. More, Y. V. H. Rao, P. I. Prasad, and B. Nageswara Rao, "Experimental investigation on the effect of compression ratio over emission and performance characteristics of the diesel engine using ternary blends," *International Journal of Green Energy*, vol. 18, no. 3, pp. 231–242, 2021, doi: 10.1080/15435075.2020.1854263.

[21] F. Polat, "Performance and emission behaviors of a CI engine fueled by waste feedstocks at varying compression ratios," *Proceedings of the Institution of Mechanical*

Engineers, Part E: Journal of Process Mechanical Engineering, vol. 236, no. 5, pp. 409-423, 2022, doi: 10.1177/09544089221074845.

[22] B. Singh and S. K. Shukla, "Experimental analysis of combustion characteristics on a variable compression ratio engine fuelled with biodiesel (castor oil) and diesel blends," *Biofuels*, vol. 7, no. 5, pp. 471–477, 2016, doi: 10.1080/17597269.2016.1163210.

[23] R. Balasubramanian and K. A. Subramanian, "Experimental investigation on the effects of compression ratio on performance, emissions and combustion characteristics of a biodiesel-fueled automotive diesel engine," *Biofuels*, vol. 12, no. 8, pp. 913–924, Feb. 2019, doi: 10.1080/17597269.2018.1558840.

[24] S. Kannan, S. Nagaraja, and N. Mathankumar, "Experimental investigation on the effect of compression ratio over the performance of corn biodiesel–diesel blends as fuel in compression ignition engine," *International Journal of Ambient Energy*, vol. 42, no. 12, pp. 1369–1377, 2020, doi: 10.1080/01430750.2020.1772871.

[25] N. F. Khanyi, F.L. Inambao, R. Stopforth, "Simulation Analysis of the Impact of Exhaust Backpressure on a Variable Compression Ratio Diesel Engine Performance," *Journal of Propulsion Technology*, vol. 46, no. 1, pp. 1178–1198, Jan. 2025.

[26] M. Anil, V. Hemadri, and M. Swamy, "Experimental investigation on impact of water-in-diesel emulsion in a single-cylinder research diesel engine," *International Journal of Ambient Energy*, vol. 43, no. 1, pp. 6088–6095, 2022, doi: 10.1080/01430750.2022.2128411.

[27] R. Pawar, S. Patil, and D. Hulwan, "Investigating the Effect of Compression Ratio on Operating Characteristics of Compression Ignition Engine Fueled with Diesel—Ricebran Biodiesel—n-Butanol Additive Blends," *J. Inst. Eng. India Ser. E*, vol. 104, pp. 129–137, 2023, doi: 10.1007/s40034-022-00264-2.

[28] S. Rehman, M. S. Nafis, M. A. Waheed, and A. A. Khan, "Experimental investigation on combustion and performance characteristics of a direct-injection diesel engine," *Int. J. Energy Clean Environ.*, vol. 23, no. 6, 2022, doi: 10.1615/interjenercleanenv.2022042597.

[29] S. Dash, P. Lingfa, and S. Chavan, "Combustion analysis of a single cylinder variable compression ratio small size agricultural DI diesel engine run by Nahar biodiesel and its diesel blends," *Energy Sources, Part A: Recovery, Utilization, and Environmental Effects*, vol. 1057, no. 1, 2020, doi: 10.1080/15567036.2019.1604878.

[30] S. Murugapoopathi and D. Vasudevan, "Experimental and numerical findings on VCR engine performance analysis on high FFA RSO biodiesel as fuel using RSM approach," *Heat and Mass Transfer*, vol. 57, no. 3, pp. 633–644, 2021, doi: 10.1007/s00231-020-02961-3.

[31] G. G. Momin, N. L. Jain, and B. A. Kumar, "The performance and emission analysis of a diesel engine using vegetable oil blends and bio-diesel as fuel – A review," *Journal of Mines, Metals and Fuels*, 2024, doi: 10.18311/jmmf/2024/45150.

[32] A. Agarwal, M. O. Dinka, and M. Ilunga, "Enhancing engine cylinder heat dissipation capacity through direct optimization (DO) techniques," *Processes*, vol. 12, no. 12, 2024, doi: 10.3390/pr12122659.

[33] A. S. Mohammed, Venkata Ramayya Ancha, Samson Mekbib Atnaw, M. Desta, and R. Bhandari, "Analysis of Cylinder Pressure and Heat Release Rate Variation in Diesel Engine Fueled with Croton Macrostachyus (CMS) Seed Oil Biodiesel as an Alternative Fuel," *Energies*, vol. 18, no. 6, pp. 1449–1449, Mar. 2025, doi: https://doi.org/10.3390/en18061449.

[34] H. O. Ghareeb and H. Abad, "Ignition Delay Period Prediction for Compression Ignition Engines Fueled with Ethanol/Diesel Blends," *Journal of Engineering*, vol. 30, no. 8, pp. 48–70, Aug. 2024, doi: https://doi.org/10.31026/j.eng.2024.08.04.

[35] A. S. Al-Shahrani, "Theoretical Analysis of Ignition in Diesel Engines," *Journal of Power and Energy Engineering*, vol. 05, no. 06, pp. 1–13, 2017, doi: https://doi.org/10.4236/jpee.2017.56001.

[36] A. T. Doppalapudi, A. K. Azad, and M. M. K. Khan, "Advanced strategies to reduce harmful nitrogen-oxide emissions from biodiesel fueled engine," *Renewable and Sustainable Energy Reviews*, vol. 174, p. 113123, Mar. 2023, doi: https://doi.org/10.1016/j.rser.2022.113123.

[37] P. Mohamed Shameer, K. Ramesh, R. Sakthivel, and R. Purnachandran, "Studies on Correlation between NOx and In-cylinder Temperature in a D.I Diesel Engine using FLUKE Thermal Imager for different Alternate Fuel Blends," *Asian Journal of Research in Social Sciences and Humanities*, vol. 6, no. 12, pp. 373–373, Jan. 2016, doi: https://doi.org/10.5958/2249-7315.2016.01298.3.

[38] S. Cong, C. David Garner, and G. McTaggart-Cowan, "The Effects of Exhaust Back Pressure on Conventional and Low-Temperature Diesel Combustion," vol. 225, no. 2, pp. 222–235, Jan. 2011, doi: https://doi.org/10.1177/09544070jauto1577.

[39] S. Zhang *et al.*, "Experimental and numerical study the effect of combustion chamber shapes on combustion and emissions characteristics in a heavy-duty lean burn SI natural gas engine coupled with detail combustion mechanism," *Fuel*, vol. 258, pp. 116130–116130, Dec. 2019, doi: https://doi.org/10.1016/j.fuel.2019.116130.

[40] I. Naruemon, L. Liu, D. Liu, X. Ma, and K. Nishida, "An analysis on the effects of the fuel injection rate shape of the diesel spray mixing process using a numerical simulation," *Applied Sciences*, vol. 10, no. 14, p. 4983, Jul. 2020, doi: 10.3390/app10144983.

[41] B. S. N. Prasad, J. K. Pandey, and G. N. Kumar, "Impact of changing compression ratio on engine characteristics of an SI engine fueled with equi-volume blend of methanol and gasoline," *Energy*, vol. 191, p. 116605, Jan. 2020, doi: 10.1016/j.energy.2019.116605.

[42] Q. Liu, B. Ma, Z. Zhang, C. Fu, and Z. Kang, "Potential Issues and Optimization Solutions for High-Compression-Ratio Utilization in Hybrid-Dedicated Gasoline Engines," *Energies*, vol. 18, no. 15, pp. 4204–4204, Aug. 2025, doi: https://doi.org/10.3390/en18154204.

[43] L. Kutej, A. Klink, S. Wegt, R. Reitz, and S. Jakirlic, "Eddy-resolving simulation of conjugate heat transfer in a test specimen pertinent to cooling channels in IC engines,"

SAE Technical Paper Series, 2024, doi: 10.4271/2024-01-2692.

[44] S. Wegt et al., "Computational Modeling of the Flow and Heat Transfer in an Internal Combustion Engine-Relevant Cooling Channel," *SAE technical paper series*, 2023, doi: 10.4271/2023-01-0198.

[45] A. Bhattad *et al.*, "Review on mono and hybrid nanofluids: Preparation, properties, investigation, and applications in IC engines and heat transfer," *Energies*, vol. 16, 2023, doi: 10.3390/en16073189.

[46] P. Duda, "Heat Transfer Coefficient Distribution—A Review of Calculation Methods," *Energies*, vol. 16, no. 9, p. 3683, Apr. 2023, doi: https://doi.org/10.3390/en16093683.

[47] L. Fonseca, P. Olmeda, R. Novella, and R. M. Valle, "Internal Combustion Engine Heat Transfer and Wall Temperature Modeling: An Overview," *Archives of Computational Methods in Engineering*, vol. 27, no. 5, pp. 1661–1679, Oct. 2019, doi: https://doi.org/10.1007/s11831-019-09361-9.

[48] R. R. Renish, A. J. Selvam, R. Čep, and M. Elangovan, "Influence of Varying Compression Ratio of a Compression Ignition Engine Fueled with B20 Blends of Sea Mango Biodiesel," *Processes*, vol. 10, no. 7, p. 1423, Jul. 2022, doi: https://doi.org/10.3390/pr10071423.

[49] T. Suzuki, Yasufumi Oguri, and M. Yoshida, "Heat Transfer in the Internal Combustion Engines," *SAE technical papers on CD-ROM/SAE technical paper series*, Mar. 2000, doi: https://doi.org/10.4271/2000-01-0300.

[50] A. Sanli, C. Sayin, M. Gumus, I. Kilicaslan, and M. Canakci, "Numerical Evaluation by Models of Load and Spark Timing Effects on the In-Cylinder Heat Transfer of a SI Engine," *Numerical Heat Transfer, Part A: Applications*, vol. 56, no. 5, pp. 444–458, Oct. 2009, doi: https://doi.org/10.1080/10407780903244312.